Acta Cryst E CRYSTALLOGRAPHIC COMMUNICATIONS

ISSN 2056-9890

Intramolecular 1,5-S···N σ-hole interaction in (*E*)-*N*′-(pyridin-4-ylmethylidene)thiophene-2-carbohydrazide

Valeri V. Mossine,[a]* Steven P. Kelley[b] and Thomas P. Mawhinney[a]

[a]Department of Biochemistry, University of Missouri, Columbia, MO 65211, USA, and [b]Department of Chemistry, University of Missouri, Columbia, MO 65211, USA. *Correspondence e-mail: mossinev@missouri.edu

Received 17 February 2020
Accepted 3 March 2020

Edited by C. Rizzoli, Universita degli Studi di Parma, Italy

Keywords: crystal structure; 4-pyridinecarboxaldehyde 2-thienyl hydrazone; chalcogen bonding; hydrogen bonding; Hirshfeld surface; intermolecular interaction energies; energy frameworks.

CCDC reference: 1983191

Supporting information: this article has supporting information at journals.iucr.org/e

The title compound, $C_{11}H_9N_3OS$, (**I**), crystallizes in the monoclinic space group $P2_1/n$. The molecular conformation is nearly planar and features an intramolecular chalcogen bond between the thiophene S and the imine N atoms. Within the crystal, the strongest interactions between molecules are the N—H···O hydrogen bonds, which organize them into inversion dimers. The dimers are linked through short C—H···N contacts and are stacked into layers propagating in the (001) plane. The crystal structure features π–π stacking between the pyridine aromatic ring and the azomethine double bond. The calculated energies of pairwise intermolecular interactions within the stacks are considerably larger than those found for the interactions between the layers.

1. Chemical context

Hydrazones are a versatile group of organic structures that have been the subject of numerous studies in chemical (Barluenga & Valdés, 2011), biomedical (Narang *et al.*, 2012), and materials (Serbutoviez *et al.*, 1995) sciences for decades. For example, hydrazone-based iron chelators have found applications as analytical reagents (Singh *et al.*, 1982) and have been proposed for the treatment of bacterial, fungal, and protozoan infections (Narang *et al.*, 2012; Rzhepishevska *et al.*, 2014), as well as health disorders involving alterations in iron metabolism, such as hemochromatosis (Jansová & Šimůnek, 2019), cancer (Lovejoy & Richardson, 2003), and neurodegenerative diseases (Richardson, 2004). In addition, since iron has been identified as a critical co-factor of bacterial phenazine cytotoxicity to mammalian host cells (Mossine *et al.*, 2016), the application of efficient iron chelators to the infection sites could not only restrict proliferation of the pathogen but also protect the infected tissue from injury caused by toxic bacterial metabolites (Mossine *et al.*, 2018).

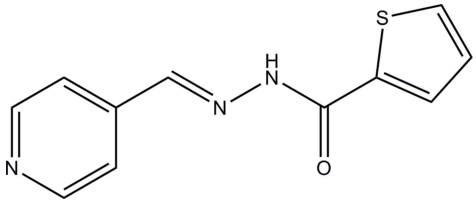

As a part of our search for potent inhibitors of cytotoxic virulence factors from drug-resistant *Pseudomonas aeruginosa*, we have prepared 4-pyridinecarboxaldehyde 2-thienyl hydrazone (**I**), a structural analog of a series of hydrazide-hydrazones that have proved to be pharmacologically active *in*

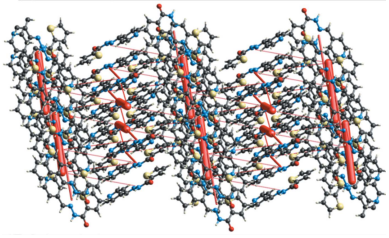

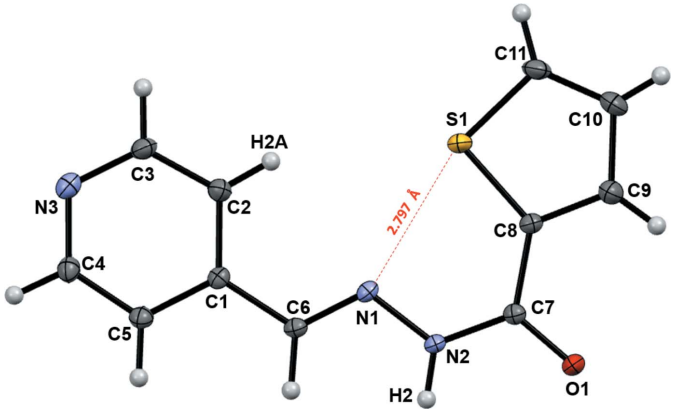

Figure 1
Atomic numbering and displacement ellipsoids at the 50% probability level for (**I**). The intramolecular chalcogen bond is shown as a dotted line.

vivo. Here we report on the molecular and crystal structures of (**I**), with an emphasis on the non-covalent interactions in the structure.

2. Structural commentary

The molecular structure and atomic numbering are shown in Fig. 1. The molecule is essentially flat, with exception of the H2 and the thiophene ring carbon and hydrogen atoms, which deviate from the molecular plane by more than 0.1 Å; the dihedral angle between the planes formed by the pyridine and the thiophene rings is only 8.28 (7)°. The configuration around the azomethine N1—C6 bond is *trans* with respect to C2 and N1, as would be expected for the structure. The conformation around the N2—C7 bond, with respect to the N1 and C8 atoms, is *cis*, however. Such a *syn*-periplanar conformation is unusual for aromatic hydrazide-hydrazones and indicates the presence of additional intramolecular interactions that could stabilize the energetically unfavorable arrangement around the amide bond. Specifically, the interatomic S1···N1 distance is 2.7971 (11) Å, which is shorter than the sum of the van der Waals radii by 0.55 Å (Table 1), thus indicating the presence of a chalcogen bond (Scilabra *et al.*, 2019). In addition, other geometric features of the molecule are in concord with the definition (Aakeroy *et al.*, 2019) of the bond. The angle between the S1—C11 σ covalent bond and the S1···N1 suspect is 164.17 (5)°, which makes the latter an extension of the former. The S1···N1—C6 angle is 148.48 (8)°, the S1 donor is in the molecular plane and approaches the N1 acceptor roughly along the axis of the lone pair. In addition, a comparison of the bond lengths in (**I**) and its structural analogues, 2-thiophene carboxylic acid (Tiekink, 1989), 2-thiophene carboxamide (Low *et al.*, 2009), or 4-hydroxybenzaldehyde 2-thienylhydrazone (Li *et al.*, 2010), which lack attractive non-covalent interactions at the sulfur atom, revealed that the S1—C11 bond in (**I**) is longer than similar bonds in the reference molecules, by 0.01–0.02 Å. The chalcogen bond is believed to originate from attractive electrostatic interactions between regions of positive ESP of a donor, such as the S1 atom, and a lone pair (or a π region) of the acceptor, such as the N1 atom in (**I**). In thiophene, two *p*-electrons of the sulfur atom participate in aromatic π-bonding, while another lone pair of *p*-electrons occupies the sp^2 orbital, with the maximum of the electron density localized in the thiophene ring plane. Nevertheless, there are regions of positive electrostatic potential, conventionally named σ-holes (Scilabra *et al.*, 2019), which are located opposite to the S—C covalent bonds. For illustrative purposes, we have calculated a distribution of the electrostatic potential over the promolecule isosurface of (**I**), which is shown in Fig. 2 and which exhibits one of the two σ-holes mapped to the surface.

Table 1
Non-covalent heteroatom interactions geometry (Å, °).

Hydrogen bonding				
D—H···*A*	*D*—H	H···*A*	*D*···*A*	*D*—H···*A*
N2—H2···O1^{i}	0.902 (18)	1.942 (18)	2.8376 (14)	171.8 (18)
C11—H11···N3^{ii}	0.936 (19)	2.501 (18)	3.3664 (18)	153.9 (14)
Chalcogen bonding				
R—*Ch*···*A*			*Ch*···*A*	*R*—*Ch*···*A*
C11—S1···N1			2.7971 (11)	164.17 (5)

Symmetry codes: (i) $1-x, -y, -z$; (ii) $2-x, 2-y, -z$.

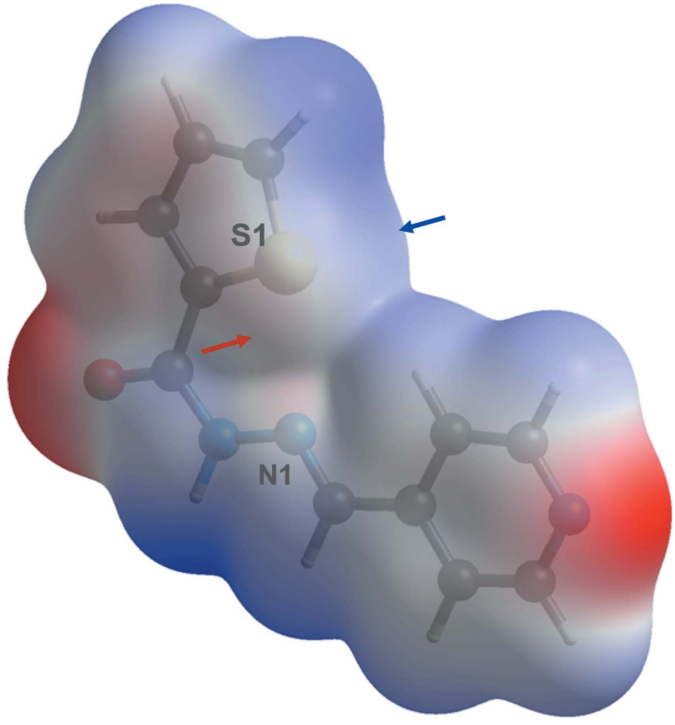

Figure 2
Electrostatic potential mapped on the promolecule 0.002 a.u. isosurface of (**I**), in the range −0.0750 to +0.0806 a.u., red indicates regions of negative ESP and blue indicates regions of positive ESP. The red arrow points at the region of negative ESP that is consistent with topography of aromatic *p*-electrons originating from the S1 atom and directed *away* from the molecular plane. The blue arrow points at the region of positive ESP associated with electronegative S1 (σ-hole) and located *within* the molecular plane. Calculations were done using a 6–311 G(d,p) basis set at the B3LYP level of theory.

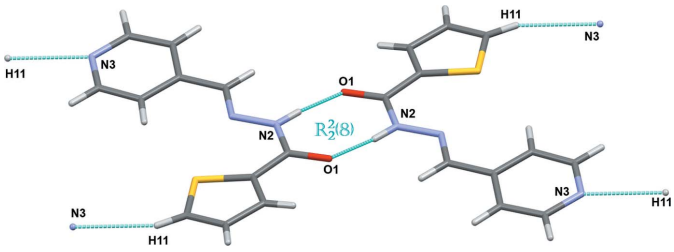

Figure 3
Hydrogen-bonded dimerization of (**I**).

3. Supramolecular features

The title compound crystallizes in the monoclinic $P2_1/n$ space group, with four equivalent molecules per unit cell. The molecules are organized pairwise as flat dimers (Fig. 3), with two hydrogen bonds of the same N2—H2···O1 type (Table 1), which are responsible for 'holding' the dimers together. This hydrogen-bonding arrangement can be described in terms of the graph-set descriptor $R_2^2(8)$. An additional pair of the short C11—H11···N3 contacts links the dimers into molecular sheets propagating in the [110] and [$\overline{1}$10] directions. The intermolecular contacts also include the π–π stacking between the pyridine aromatic ring and the azomethine double bond.

To evaluate the contributions of these and other intermolecular contacts to the energetics of the crystal lattice in (**I**), we calculated pairwise interaction energies for all unique contacts found in the crystal structure. The results are shown in Fig. 4. It follows from these data that electrostatic interactions within the dimers are the major contributors to the packing forces in the crystal of (**I**). The *Crystal Explorer* software (Spackman *et al.*, 2008) provides a tool to illustrate the magnitude and directionality of the major interactions within a crystal structure, the energy frameworks builder (Turner *et al.*, 2015). Using the pairwise interaction energies calculated for (**I**), we obtained energy framework diagrams for the contributions of electrostatic and dispersion forces, as well as for the total energy. The diagrams and crystal packing are shown in Fig. 5. According to the diagrams, the main crystal packing forces are those that form sheets of the dimers, as well as stacks of the sheets. These stacks are organized in layers that are about 10 Å thick and run in parallel to (001). Intermolecular contacts between molecules located in neighboring layers are weak.

4. Database survey

The crystal structures of three metal complexes, containing 4-pyridinecarboxaldehyde 2-thienylhydrazone coordinated to copper(I) triphenylphosphinate, have been published [CSD (Groom *et al.*, 2016) refcodes CCDC 1401340, 1433202, 1433203; Gholivand *et al.*, 2016], but the crystal structure of

(*a*)

(*b*)

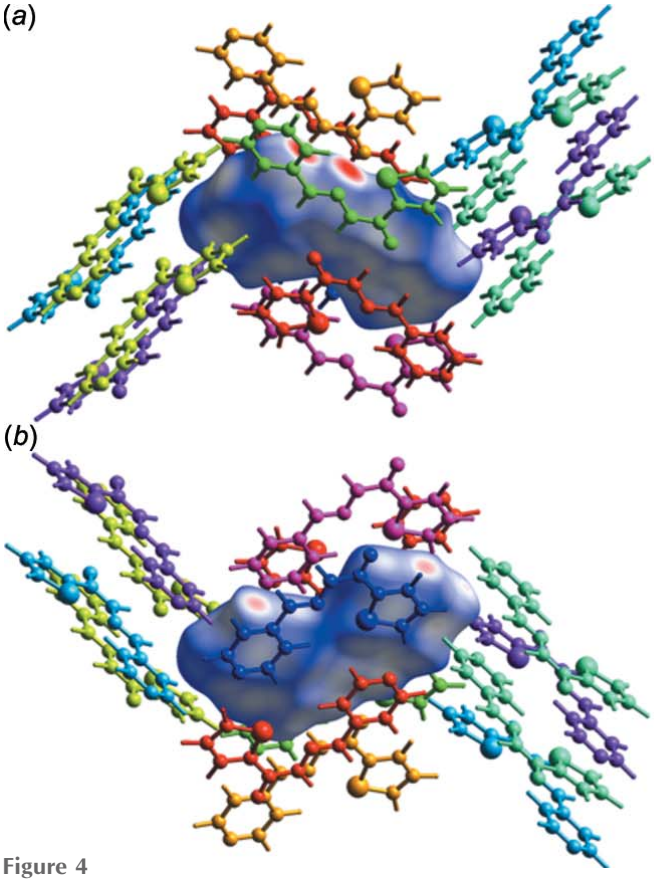

(*c*)

Pairwise interactions energies (kJ/mol)
B3LYP/6-31G(d,p) electron densities energy model

Color code	N	Symm operator	E elstat	E polar	E disp	E repuls	E total
	2	x, y, z	-3.0	-3.3	-59.4	41.6	-31.6
	1	-x, -y, -z	-99.9	-23.6	-19.2	105.5	-74.6
	2	-x+1/2, y+1/2, -z+1/2	-4.7	-0.7	-10.2	6.3	-10.5
	1	-x, -y, -z	-11.3	-6.3	-29.3	17.9	-31.0
	2	-x+1/2, y+1/2, -z+1/2	-6.2	-1.2	-11.3	9.1	-11.7
	2	x+1/2, -y+1/2, z+1/2	1.8	-0.5	-4.1	1.0	-1.4
	1	-x, -y, -z	-2.0	-0.8	-20.2	10.2	-14.0
	2	x+1/2, -y+1/2, z+1/2	-0.9	-0.7	-10.8	8.1	-5.9
	1	-x, -y, -z	-24.9	-5.8	-22.8	36.6	-27.8

Figure 4
Interaction energies in crystal structure of (**I**). (*a*), (*b*) Views of interactions between a central molecule, shown as its Hirshfeld surface, and 14 molecules that share the interaction surfaces with the central molecule. (*c*) Calculated energies (electrostatic, polarization, dispersion, repulsion, and total) of pairwise interactions between the central molecule and those indicated by respective colors.

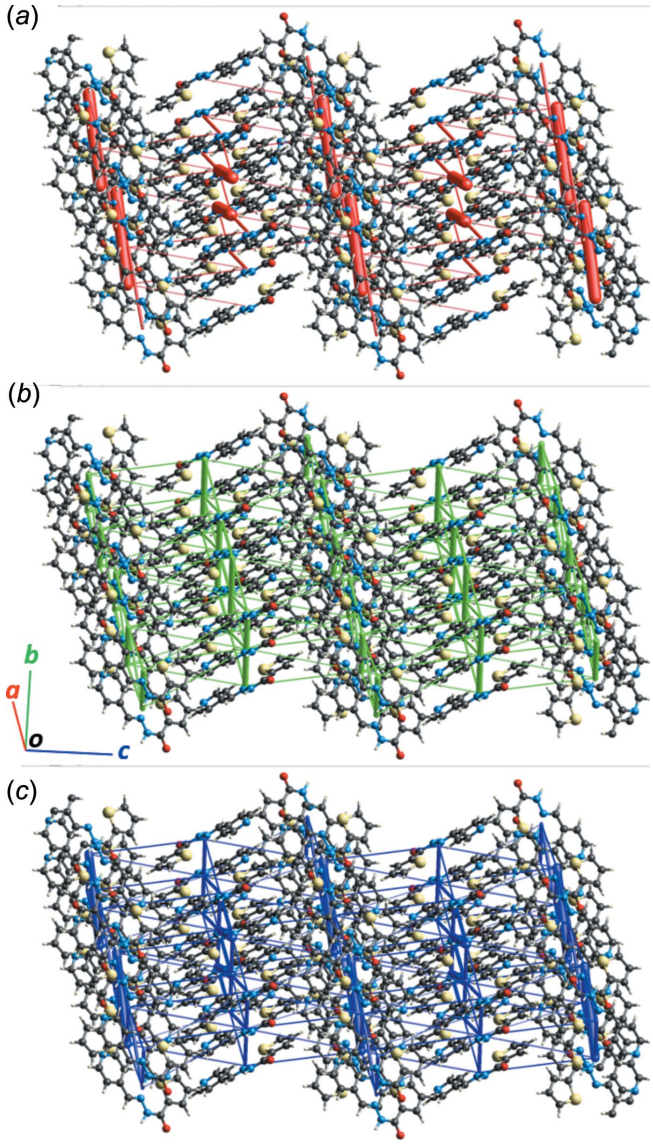

Figure 5
Energy frameworks for separate (*a*) electrostatic and (*b*) dispersion contributions to the (*c*) total pairwise interaction energies. The cylinders link molecular centroids, and the cylinder thickness is proportional to the magnitude of the energies (see Fig. 4). For clarity, the cylinders corresponding to energies <5 kJ mol^{-1} are not shown. The directionality of the crystallographic axes is the same for all three diagrams.

the title compound as a single molecule has not been reported previously. In the same paper, the copper complexes of 2-pyridinecarboxaldehyde 2-thienylhydrazone (CCDC 1433200) and 3-pyridinecarboxaldehyde 2-thienylhydrazone (CCDC 1433201) were also reported. In four complexes, molecules of 3- or 4-pyridinecarboxaldehyde 2-thienylhydrazone act as monodentate ligands bound to the copper ion through the pyridine nitrogens, are not ionized and do assume conformations close to that of free (**I**), thus suggesting that the intramolecular chalcogen bonding is retained if coordination to the metal occurs *via* a remote part of the molecule. In contrast, 2-pyridinecarboxaldehyde 2-thienylhydrazone was found to chelate Cu^{+} through the pyridine and the imine nitrogen atoms, so that the chalcogen bonding between the thiophene sulfur and the imine nitrogen atoms was disabled. The dimer-forming hydrogen bonding did survive in the CCDC 1433201, 1433202 and 1433203 structures as well. Not only a coordinated metal ion, such as the aforementioned copper in CCDC 1433200, but also an opportunistic hydrogen bonding can disable the chalcogen bonding in 2-thiophenecarboxylic acid-derived hydrazide-hydrazones. For instance, crystalline Schiff bases of 2-thiophenecarboxylic acid hydrazide and 4-methoxybenzaldehyde (Li & Jian, 2010), or 2-acetylpyridine (Christidis *et al.*, 1995) adopt conformations similar to (**I**), thus suggesting a general trend of 1,5-S$\cdots$N chalcogen-bond formation in structures analogous to (**I**). In contrast, in hydrazones formed by condensation of 2-thiophenecarboxylic acid hydrazide and 4-hydroxybenzaldehyde (Li *et al.*, 2010) or 2-hydroxyacetophenone (Jiang, 2011; Singh *et al.*, 2013), which have an additional hydrogen-bonding interaction between the aromatic hydroxyl groups and the imine nitrogen, the intramolecular chalcogen bonding is switched to a weaker 1,4-S$\cdots$O$_{\text{carbonyl}}$ contact.

Table 2
Experimental details.

Crystal data	
Chemical formula	$C_{11}H_9N_3OS$
M_r	231.27
Crystal system, space group	Monoclinic, $P2_1/n$
Temperature (K)	100
a, b, c (Å)	12.0600 (8), 4.4531 (3), 19.9528 (13)
β (°)	102.228 (2)
V (Å^3)	1047.24 (12)
Z	4
Radiation type	Mo $K\alpha$
μ (mm^{-1})	0.29
Crystal size (mm)	0.49 × 0.04 × 0.01
Data collection	
Diffractometer	Bruker APEXII CCD
Absorption correction	Multi-scan (*AXScale*; Bruker, 2016)
T_{min}, T_{max}	0.694, 0.746
No. of measured, independent and observed [$I > 2\sigma(I)$] reflections	25531, 3767, 2821
R_{int}	0.059
(sin $\theta/\lambda)_{max}$ (Å^{-1})	0.754
Refinement	
$R[F^2 > 2\sigma(F^2)]$, $wR(F^2)$, S	0.040, 0.101, 1.03
No. of reflections	3767
No. of parameters	172
H-atom treatment	Only H-atom coordinates refined
$\Delta\rho_{max}$, $\Delta\rho_{min}$ (e Å^{-3})	0.44, −0.29

Computer programs: *APEX3* and *SAINT* (Bruker, 2016), *SHELXS* (Sheldrick, 2008), *SHELXL* (Sheldrick, 2015), *OLEX2*(Dolomanov *et al.*, 2009), *Mercury* (Macrae *et al.*, 2020) and *publCIF* (Westrip, 2010).

5. Synthesis and crystallization

To a suspension of 2-thiophenecarboxylic acid hydrazide (711 mg, 5 mmol) in 15 mL of 70% aqueous EtOH were added 0.536 mg (471 µL, 5 mmol) of 4-pyridinecarboxaldehyde, and the reaction mixture was stirred for 2 h at 343 K. The resulting clear solution was brought to 277 K and left for two days to

crystallize as colorless needles. Suitable crystals were then selected for subsequent diffraction studies.

6. Refinement details

Crystal data, data collection and structure refinement details are summarized in Table 2. All H-atom coordinates were refined freely.

Funding information

Funding for this research was provided by: University of Missouri Agriculture Experiment Station Chemical Laboratories; National Institute of Food and Agriculture (grant No. MO-HABC0002).

References

Aakeroy, C. B., Bryce, D. L., Desiraju, G. R., Frontera, A., Legon, A. C., Nicotra, F., Rissanen, K., Scheiner, S., Terraneo, G., Metrangolo, P. & Resnati, G. (2019). *Pure Appl. Chem.* **91**, 1889–1892.
Barluenga, J. & Valdés, C. (2011). *Angew. Chem. Int. Ed.* **50**, 7486–7500.
Bruker (2016). *APEX3*, *SAINT* and *AXScale*. Bruker AXS Inc., Madison, Wisconsin, USA.
Christidis, P. C., Tossidis, I. A. & Hondroudis, C. A. (1995). *Z. Kristallogr.* **210**, 373.
Dolomanov, O. V., Bourhis, L. J., Gildea, R. J., Howard, J. A. K. & Puschmann, H. (2009). *J. Appl. Cryst.* **42**, 339–341.
Gholivand, K., Farshadfer, K., Roe, S. M., Gholami, A. & Esrafili, M. D. (2016). *CrystEngComm*, **18**, 2873–2884.
Groom, C. R., Bruno, I. J., Lightfoot, M. P. & Ward, S. C. (2016). *Acta Cryst.* B**72**, 171–179.
Jansová, H. & Šimůnek, T. (2019). *Curr. Med. Chem.* **26**, 288–301.
Jiang, J.-H. (2011). *Acta Cryst.* E**67**, o32.
Li, Y.-F. & Jian, F.-F. (2010). *Acta Cryst.* E**66**, o1400.
Li, Y.-F., Jiang, J.-H. & Jian, F.-F. (2010). *Acta Cryst.* E**66**, o1719.
Lovejoy, D. B. & Richardson, D. R. (2003). *Curr. Med. Chem.* **10**, 1035–1049.
Low, J. N., Quesada, A., Santos, L. M. N. B. F., Schröder, B. & Gomes, L. R. (2009). *J. Chem. Crystallogr.* **39**, 747–752.
Macrae, C. F., Sovago, I., Cottrell, S. J., Galek, P. T. A., McCabe, P., Pidcock, E., Platings, M., Shields, G. P., Stevens, J. S., Towler, M. & Wood, P. A. (2020). *J. Appl. Cryst.* **53**, 226–235.
Mossine, V. V., Chance, D. L., Waters, J. K. & Mawhinney, T. P. (2018). *Antimicrob. Agents Chemother.* **62**, e02349.
Mossine, V. V., Waters, J. K., Chance, D. L. & Mawhinney, T. P. (2016). *Toxicol. Sci.* **154**, 403–415.
Narang, R., Narasimhan, B. & Sharma, S. (2012). *Curr. Med. Chem.* **19**, 569–612.
Richardson, D. R. (2004). *Ann. N. Y. Acad. Sci.* **1012**, 326–341.
Rzhepishevska, O., Hakobyan, S., Ekstrand-Hammarström, B., Nygren, Y., Karlsson, T., Bucht, A., Elofsson, M., Boily, J.-F. & Ramstedt, M. (2014). *J. Inorg. Biochem.* **138**, 1–8.
Scilabra, P., Terraneo, G. & Resnati, G. (2019). *Acc. Chem. Res.* **52**, 1313–1324.
Serbutoviez, C., Bosshard, C., Knoepfle, G., Wyss, P., Pretre, P., Guenter, P., Schenk, K., Solari, E. & Chapuis, G. (1995). *Chem. Mater.* **7**, 1198–1206.
Sheldrick, G. M. (2008). *Acta Cryst.* A**64**, 112–122.
Sheldrick, G. M. (2015). *Acta Cryst.* C**71**, 3–8.
Singh, P., Singh, A. K. & Singh, V. P. (2013). *Polyhedron*, **65**, 73–81.
Singh, R. B., Jain, P. & Singh, R. P. (1982). *Talanta*, **29**, 77–84.
Spackman, M. A., McKinnon, J. J. & Jayatilaka, D. (2008). *CrystEngComm*, **10**, 377–388.
Tiekink, E. R. T. (1989). *Z. Kristallogr.* **188**, 307–310.
Turner, M. J., Thomas, S. P., Shi, M. W., Jayatilaka, D. & Spackman, M. A. (2015). *Chem. Commun.* **51**, 3735–3738.
Westrip, S. P. (2010). *J. Appl. Cryst.* **43**, 920–925.

supporting information

Acta Cryst. (2020). E**76**, 557-561 [https://doi.org/10.1107/S2056989020003011]

Intramolecular 1,5-S···N σ-hole interaction in (*E*)-*N*′-(pyridin-4-ylmethylidene)thiophene-2-carbohydrazide

Valeri V. Mossine, Steven P. Kelley and Thomas P. Mawhinney

Computing details

Data collection: *SAINT* (Bruker, 2016); cell refinement: *APEX3* (Bruker, 2016); data reduction: *SAINT* (Bruker, 2016); program(s) used to solve structure: *SHELXS* (Sheldrick, 2008); program(s) used to refine structure: *SHELXL* (Sheldrick, 2015); molecular graphics: *OLEX2*(Dolomanov *et al.*, 2009), *Mercury* (Macrae *et al.*, 2020); software used to prepare material for publication: *publCIF* (Westrip, 2010).

(*E*)-*N*′-(Pyridin-4-ylmethylidene)thiophene-2-carbohydrazide

Crystal data

$C_{11}H_9N_3OS$
$M_r = 231.27$
Monoclinic, $P2_1/n$
$a = 12.0600$ (8) Å
$b = 4.4531$ (3) Å
$c = 19.9528$ (13) Å
$\beta = 102.228$ (2)°
$V = 1047.24$ (12) Å^3
$Z = 4$
$F(000) = 480$
$D_x = 1.467$ Mg m^{-3}
Mo $K\alpha$ radiation, $\lambda = 0.71073$ Å
Cell parameters from 8101 reflections
$\theta = 2.2$–$32.3°$
$\mu = 0.29$ mm^{-1}
$T = 100$ K
Needle, clear colourless
0.49 × 0.04 × 0.01 mm

Data collection

Bruker APEXII CCD diffractometer
Radiation source: Sealed Source Mo with TRIUMPH optics
Graphite monochromator
ω and phi scans
Absorption correction: multi-scan (*AXScale*; Bruker, 2016)
$T_{min} = 0.694$, $T_{max} = 0.746$
25531 measured reflections
3767 independent reflections
2821 reflections with $I > 2\sigma(I)$
$R_{int} = 0.059$
$\theta_{max} = 32.4°$, $\theta_{min} = 2.2°$
$h = -18\rightarrow18$
$k = -6\rightarrow6$
$l = -30\rightarrow30$

Refinement

Refinement on F^2
Least-squares matrix: full
$R[F^2 > 2\sigma(F^2)] = 0.040$
$wR(F^2) = 0.101$
$S = 1.03$
3767 reflections
172 parameters
0 restraints
Hydrogen site location: difference Fourier map
Only H-atom coordinates refined
$w = 1/[\sigma^2(F_o^2) + (0.0482P)^2 + 0.4155P]$ where $P = (F_o^2 + 2F_c^2)/3$
$(\Delta/\sigma)_{max} < 0.001$
$\Delta\rho_{max} = 0.44$ e Å^{-3}
$\Delta\rho_{min} = -0.28$ e Å^{-3}

Special details

Geometry. All esds (except the esd in the dihedral angle between two l.s. planes) are estimated using the full covariance matrix. The cell esds are taken into account individually in the estimation of esds in distances, angles and torsion angles; correlations between esds in cell parameters are only used when they are defined by crystal symmetry. An approximate (isotropic) treatment of cell esds is used for estimating esds involving l.s. planes.

Fractional atomic coordinates and isotropic or equivalent isotropic displacement parameters (Å²)

	x	*y*	*z*	U_{iso}*/U_{eq}
S1	0.86385 (3)	0.41227 (8)	0.09663 (2)	0.01759 (9)
O1	0.57985 (7)	−0.0566 (2)	0.08737 (5)	0.01585 (19)
N1	0.67837 (8)	0.4814 (2)	−0.01319 (5)	0.0121 (2)
C3	0.86828 (11)	1.1139 (3)	−0.10148 (7)	0.0177 (3)
C6	0.63662 (10)	0.6002 (3)	−0.07173 (6)	0.0123 (2)
N2	0.61184 (9)	0.2710 (2)	0.00868 (5)	0.0125 (2)
C8	0.75495 (10)	0.1986 (3)	0.11541 (6)	0.0128 (2)
C7	0.64471 (10)	0.1304 (3)	0.06997 (6)	0.0119 (2)
N3	0.82339 (9)	1.2476 (3)	−0.16131 (6)	0.0170 (2)
C1	0.70133 (10)	0.8252 (3)	−0.10079 (6)	0.0117 (2)
C10	0.89639 (12)	0.1627 (4)	0.21440 (7)	0.0214 (3)
C2	0.81256 (10)	0.9054 (3)	−0.06925 (7)	0.0158 (2)
C9	0.78539 (11)	0.0796 (3)	0.18034 (7)	0.0191 (3)
C5	0.65308 (11)	0.9644 (3)	−0.16254 (6)	0.0146 (2)
C4	0.71673 (11)	1.1716 (3)	−0.19047 (7)	0.0162 (2)
C11	0.94837 (11)	0.3405 (3)	0.17495 (7)	0.0190 (3)
H2	0.5467 (15)	0.214 (4)	−0.0197 (9)	0.023*
H6	0.5592 (15)	0.543 (4)	−0.0981 (9)	0.023*
H5	0.5756 (15)	0.918 (4)	−0.1848 (9)	0.023*
H2A	0.8487 (14)	0.813 (4)	−0.0278 (9)	0.023*
H4	0.6850 (14)	1.273 (4)	−0.2329 (9)	0.023*
H9	0.7381 (14)	−0.038 (4)	0.1991 (9)	0.023*
H3	0.9464 (15)	1.168 (4)	−0.0810 (9)	0.023*
H11	1.0212 (15)	0.424 (4)	0.1851 (9)	0.023*
H10	0.9262 (15)	0.103 (4)	0.2563 (9)	0.023*

Atomic displacement parameters (Å²)

	U^{11}	U^{22}	U^{33}	U^{12}	U^{13}	U^{23}
S1	0.01205 (14)	0.02312 (18)	0.01612 (15)	−0.00603 (12)	−0.00037 (11)	0.00258 (13)
O1	0.0135 (4)	0.0181 (5)	0.0154 (4)	−0.0049 (3)	0.0018 (3)	0.0027 (4)
N1	0.0121 (4)	0.0104 (5)	0.0142 (5)	−0.0024 (4)	0.0038 (4)	−0.0003 (4)
C3	0.0130 (5)	0.0181 (6)	0.0217 (6)	−0.0037 (5)	0.0030 (5)	0.0006 (5)
C6	0.0109 (5)	0.0115 (5)	0.0141 (5)	−0.0010 (4)	0.0022 (4)	−0.0012 (5)
N2	0.0106 (4)	0.0129 (5)	0.0131 (5)	−0.0036 (4)	0.0008 (4)	0.0012 (4)
C8	0.0108 (5)	0.0133 (5)	0.0140 (5)	−0.0018 (4)	0.0021 (4)	−0.0006 (5)
C7	0.0112 (5)	0.0114 (6)	0.0130 (5)	0.0001 (4)	0.0025 (4)	−0.0007 (4)
N3	0.0178 (5)	0.0156 (5)	0.0189 (5)	−0.0027 (4)	0.0069 (4)	−0.0006 (4)
C1	0.0131 (5)	0.0100 (5)	0.0127 (5)	−0.0002 (4)	0.0040 (4)	−0.0014 (4)

C10	0.0176 (6)	0.0279 (7)	0.0158 (6)	−0.0019 (5)	−0.0034 (5)	0.0021 (5)
C2	0.0136 (5)	0.0160 (6)	0.0170 (6)	−0.0008 (5)	0.0011 (4)	0.0019 (5)
C9	0.0162 (6)	0.0244 (7)	0.0156 (6)	−0.0033 (5)	0.0010 (5)	0.0023 (5)
C5	0.0150 (5)	0.0146 (6)	0.0139 (5)	−0.0018 (4)	0.0022 (4)	−0.0013 (5)
C4	0.0205 (6)	0.0152 (6)	0.0134 (5)	−0.0017 (5)	0.0043 (5)	0.0005 (5)
C11	0.0118 (5)	0.0246 (7)	0.0183 (6)	−0.0021 (5)	−0.0018 (5)	−0.0017 (5)

Geometric parameters (Å, º)

S1—C11	1.7055 (14)	C8—C7	1.4736 (16)
S1—C8	1.7259 (12)	N3—C4	1.3381 (17)
O1—C7	1.2410 (15)	C1—C5	1.3918 (17)
N1—C6	1.2839 (16)	C1—C2	1.4019 (17)
N1—N2	1.3643 (14)	C10—C11	1.360 (2)
C3—N3	1.3413 (18)	C10—C9	1.4161 (19)
C3—C2	1.3821 (18)	C10—H10	0.879 (17)
C3—H3	0.974 (17)	C2—H2A	0.944 (17)
C6—C1	1.4631 (17)	C9—H9	0.912 (18)
C6—H6	1.002 (17)	C5—C4	1.3900 (18)
N2—C7	1.3561 (15)	C5—H5	0.968 (17)
N2—H2	0.901 (18)	C4—H4	0.963 (17)
C8—C9	1.3756 (18)	C11—H11	0.936 (18)
C11—S1—C8	91.85 (6)	C2—C1—C6	122.44 (11)
C6—N1—N2	115.48 (10)	C11—C10—C9	112.28 (12)
N3—C3—C2	124.61 (12)	C11—C10—H10	125.6 (12)
N3—C3—H3	115.8 (10)	C9—C10—H10	122.2 (12)
C2—C3—H3	119.5 (10)	C3—C2—C1	118.39 (12)
N1—C6—C1	120.21 (11)	C3—C2—H2A	121.5 (10)
N1—C6—H6	121.1 (10)	C1—C2—H2A	120.1 (10)
C1—C6—H6	118.7 (10)	C8—C9—C10	112.84 (12)
C7—N2—N1	121.75 (10)	C8—C9—H9	122.8 (11)
C7—N2—H2	119.0 (11)	C10—C9—H9	124.3 (11)
N1—N2—H2	119.0 (11)	C4—C5—C1	119.19 (12)
C9—C8—C7	121.75 (11)	C4—C5—H5	121.3 (10)
C9—C8—S1	110.68 (9)	C1—C5—H5	119.5 (10)
C7—C8—S1	127.51 (9)	N3—C4—C5	123.72 (12)
O1—C7—N2	118.73 (11)	N3—C4—H4	115.5 (10)
O1—C7—C8	120.41 (11)	C5—C4—H4	120.8 (10)
N2—C7—C8	120.86 (11)	C10—C11—S1	112.35 (10)
C4—N3—C3	116.38 (11)	C10—C11—H11	129.3 (11)
C5—C1—C2	117.70 (11)	S1—C11—H11	118.3 (11)
C5—C1—C6	119.85 (11)		

Hydrogen-bond geometry (Å, °)

D-H···*A*	*D*-H	H···*A*	D···*A*	D-H···*A*
N2-H2···O1^{i}	0.902 (18)	1.942 (18)	2.8376 (14)	171.8 (18)

C11-H11···N3^{ii}	0.936 (19)	2.501 (18)	3.3664 (18)	153.9 (14)

Symmetry codes: (i) 1-x,-y,-z; (ii) 2-x,2-y,-z